Journal of Alloys and Compounds 696 (2017) 844–849

Contents lists available at ScienceDirect

Journal of Alloys and Compounds

journal homepage: http://www.elsevier.com/locate/jalcom

CrN thin films with ultra-low magnetoresistance prepared via solution processing for large-area applications

Zhenzhen Hui [a, b, 1], Qiumin Meng [c, d, 1], Renhuai Wei [a], Xianwu Tang [a], Xiangde Zhu [c], Zhengrong Ouyang [c], Jianming Dai [a], Wenhai Song [a], Hongmei Luo [e], Xuebin Zhu [a, *], Yuping Sun [a, c, **]

[a] Key Laboratory of Materials Physics, Institute of Solid State Physics, Chinese Academy of Sciences, Hefei, 230031, China
[b] College of Chemistry and Materials Engineering, Anhui Science and Technology University, Fengyang, 233100, China
[c] High Magnetic Field Laboratory, Chinese Academy of Sciences, Hefei, 230031, China
[d] University of Science and Technology of China, Hefei, China
[e] Department of Chemical and Materials Engineering, New Mexico State University, Las Cruces, NM, 88003, USA

ARTICLE INFO

Article history:
Received 22 July 2016
Received in revised form
2 December 2016
Accepted 5 December 2016
Available online 7 December 2016

Keywords:
Chemical solution deposition
Thin films
Temperature sensors
High magnetic fields

ABSTRACT

CrN thin films are versatile in lots of applications. To develop a facile processing method for large-area CrN thin films with low-cost is unquestionable to improve the technical advances in CrN applications. In this work, CrN thin films are prepared by chemical solution deposition processing for large-area applications. The electrical transport properties are investigated, showing semiconductor-like properties. Magnetoresistance at low temperatures under high magnetic fields is observed in the CrN thin films, showing ultra-low magnetoresistance under 14T of −0.14% and −0.10% at 4.2 and 2 K, respectively.

1. Introduction

CrN thin films have attracted much interest due to their excellent performance in applications such as hard protective coatings on cutting tools, diffusion barriers, wear resistant electrical contacts and thermoelectric materials [1,2]. Up to now, several methods have been successfully used to prepare CrN thin films including reactive magnetron sputtering, pulsed laser deposition, arc evaporation, radio-frequency plasma-assisted molecular beam epitaxy, ion beam assisted deposition and so on [3–8]. To develop a facile processing method for large-area CrN thin films with low-cost is unquestionable to improve the technical advances in CrN applications. As an alternative approach for thin film preparation, chemical solution deposition (CSD) will offer advantages in terms of low-cost, atomic-scale mixing and coating of large-area onto arbitrary surface [9–14].

In contrast with the well-known magnetic properties, the transport properties of CrN thin films show controversial results. Some reported that the transport properties of CrN thin films show a metallic conductivity accompanied with a steep change around the *Néel* temperature with the resistivity range of 0.3–1.7 mΩ cm at 300 K, and the electrical transport behaviors match well with the structural transition [4,15]. Some others reported that the transport properties of CrN thin films are semiconductor-like with the resistivity range of 3.5×10^2 to 3×10^5 mΩ cm at 300 K. The differences of transport properties are usually attributed to the large differences in stoichiometry and/or microstructures including grain size, porosity and defect concentration [16,17]. On the other hand, magnetoresistance ($MR=(\rho_H-\rho_0)/\rho_0 \times 100\%$, where ρ_H and ρ_0 is the resistivity with and without an applied magnetic field, respectively) in CrN is rarely reported. In fact, materials with ultra-low *MR* (*ULMR*) at low temperatures are needed more and more to carry out temperature measurements with high magnetic field technology developments. Recently, *ULMR* is preliminarily observed in CrN thin films, which shed light on possible applications as resistance thin film temperature sensors at low temperatures in high magnetic

* Corresponding author.
** Corresponding author. Key Laboratory of Materials Physics, Institute of Solid State Physics, Chinese Academy of Sciences, Hefei, 230031, China.
E-mail addresses: xbzhu@issp.ac.cn (X. Zhu), ypsun@issp.ac.cn (Y. Sun).
[1] This two authors contribute equally.

http://dx.doi.org/10.1016/j.jallcom.2016.12.048
0925-8388/

fields [18–20].

Herein, polycrystalline CrN thin films are prepared by optimized CSD processing. The annealing temperature effects on microstructures as well as transport properties are investigated. The results show that the prepared CrN thin films show semiconductor-like electrical transport properties, and especially *ULMR* is observed under applied magnetic field of 14T at low temperatures, suggesting CrN thin films can be considered as potential, low-cost, thin film resistance temperature sensors in high magnetic fields.

2. Experimental details

2.1. Synthesis of CrN thin films by chemical solution deposition

Here, as compared with our previous report [18] an optimized CSD processing is carried out for CrN thin films. $Cr(NO_3)_3 \cdot 9H_2O$ was dissolved into 2-methoxyethanaol (2-MOE) at 80 °C, and stirred at this temperature for 20 min, and then stirred at room temperature for more than 6 h to get well mixed solution. The mixed solution was adjusted to a concentration of 0.4 M in CrN. The usage of 2-MOE instead of ammonia water and acetic acid will improve the wettability between the solution and the substrates as compared with our previous report [18]. Before the deposition processing, all the $SrTiO_3$ (100) single crystal substrates were ultrasonically cleaned subsequently with acetone, ethyl alcohol and deionized water, and then cleaned in a plasma-cleaner for 10 min. All the thin films were deposited by a spin coater with a rotation speed of 5000 rpm and a time of 10 s, and baked in air at 150 °C for 2 min and then baked in air at 350 °C for 10 min. In order to enhance the thickness, the above processing was repeated. Finally, the baked films were annealed at different temperatures for 2 h under a flowing ammonia atmosphere with 1 atm pressure. Here, as compared with our previous report [18], the pyrolysis processing under the mixture of hydrogen and nitrogen atmosphere at 500 °C is discarded, which will lead to a smaller grain size and is beneficial for the atom diffusion resulting in high quality CrN thin films.

2.2. Characterizations and measurements of the obtained thin films

The crystal phase and quality were analyzed by X-ray Diffraction (XRD) using Cu-$K_\alpha\alpha$ radiation on a Philips X'pert Pro machine (Nickel filter and Bragg-Brentano geometry, PANalytical B. V., Almelo, Netherlands). The surface morphology and the film thickness were determined using a Field-Emission Scanning Electron Microscope (FE-SEM, FEI Sirion 200). The crystallite size and the crystalline quality were also checked using a Transmission Electron Microscope (TEM, JEM-2010). The chemical states of Cr and N were analyzed by an X-ray Photoelectron Spectrometer using Al-K_α source gun (XPS, ESCALAB250). Electrical transport properties were measured on a Physical Property Measurement System (PPMS, Quantum Design) using the standard four-point probe technique. The room-temperature Hall measurements were also carried out on the PPMS using the van der Pauw geometry.

3. Results and discussion

3.1. Crystal structure and surface morphology

Fig. 1 shows the Grazing Incidence XRD (GIXRD) patterns for all the CrN thin films annealed under different temperatures. All the thin films are polycrystalline due to the large lattice mismatch ($\varepsilon = (a_f\text{-}a_s)/a_f \times 100\%$, a_f and a_s is the lattice constant of the thin film and the substrate, respectively) between the CrN thin film (a_f ~ 4.13 to 4.15 Å) and the $SrTiO_3$ substrate (a_s = 3.90 Å). Shown in Fig. 1, it is seen that the thin film annealed at 700 °C (T700) consists of two

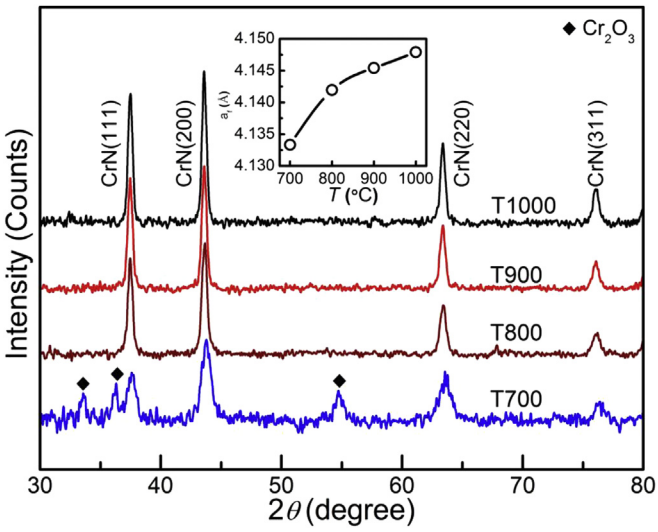

Fig. 1. Grazing incidence XRD of CrN thin films annealed at different temperatures. The annealing temperature dependence of lattice constants is shown in the inset.

phases, naming the phases of Cr_2O_3 and CrN. As for the thin film annealed at 800 °C (T800) phase-pure CrN thin film is achieved. With the increasing annealing temperature to 900 (T900) and 1000 °C (T1000), the intensity of the CrN diffraction peaks is enhanced, suggesting the improved crystalline quality. The lattice constant a_f is calculated by Bragg formula and the results are shown in the inset of Fig. 1. The a_f is determined as 4.133(2), 4.142(2), 4.145(2) and 4.148(2) Å for the T700, T800, the T900 and the T1000 thin films, respectively. The determined values are within the scope of the reported lattice constants of CrN and the slight variation in a_f can be attributed to different N content in the prepared CrN thin films. As reported previously, the more N content, the larger a_f is [21]. Additionally, the obtained a_f of 4.148(2) Å for the T1000 is in very good agreement with the stoichiometric CrN with lattice constant of 4.149 Å, suggesting the near stoichiometry of the T1000 [21].

As for the reaction mechanisms, $Cr(NO_3)_3$ is decomposed into Cr_2O_3 after baked in air as depicted by $Cr(NO_3)_3 + O_2 \xrightarrow{350\ ^\circ C} Cr_2O_3$, which is also confirmed in our experiments [22]. With the increasing annealing temperature up to 700 °C, ammonia is decomposed into N_2 and H_2 as $NH_3 \xrightarrow{\geq 700\ ^\circ C} N_2 + H_2$ [22]. Then, Cr_2O_3 will be reacted with H_2 and N_2 as $Cr_2O_3 + H_2 \xrightarrow{\geq 700\ ^\circ C} Cr$ and $Cr + N_2 \xrightarrow{\geq 700\ ^\circ C} CrN$. The reactions between Cr_2O_3 and NH_3 are preceded by a diffusion model [22]. At 700 °C, the surface Cr_2O_3 grains start to be reduced into Cr by H_2 and then Cr will react with N_2 to form CrN phase. The appearance of CrN phase at 700 °C is same as the previous report [23]. However, at this temperature the inner Cr_2O_3 particles cannot be fully reduced, resulting in the appearance of Cr_2O_3. With the further increasing annealing temperature, the activity of H_2 and N_2 are largely improved [24], resulting in the accelerated chemical reactions and the phase-pure CrN thin films as observed in XRD results.

The prepared CrN thin films show metallic gloss with gold color and the photograph of the T1000 thin film as a typical sample is presented in Fig. 2(a), showing homogenous surface morphology. Fig. 2(b), (c) and (d) show the surface FE-SEM results of the CrN thin films annealed at different temperatures, showing relatively smooth and dense surfaces. To obtain the average grain size, several hundreds of grains are examined using an image analyzer. The grain size distribution of each film is shown by a histogram in the corresponding FE-SEM results. The average grain size is determined

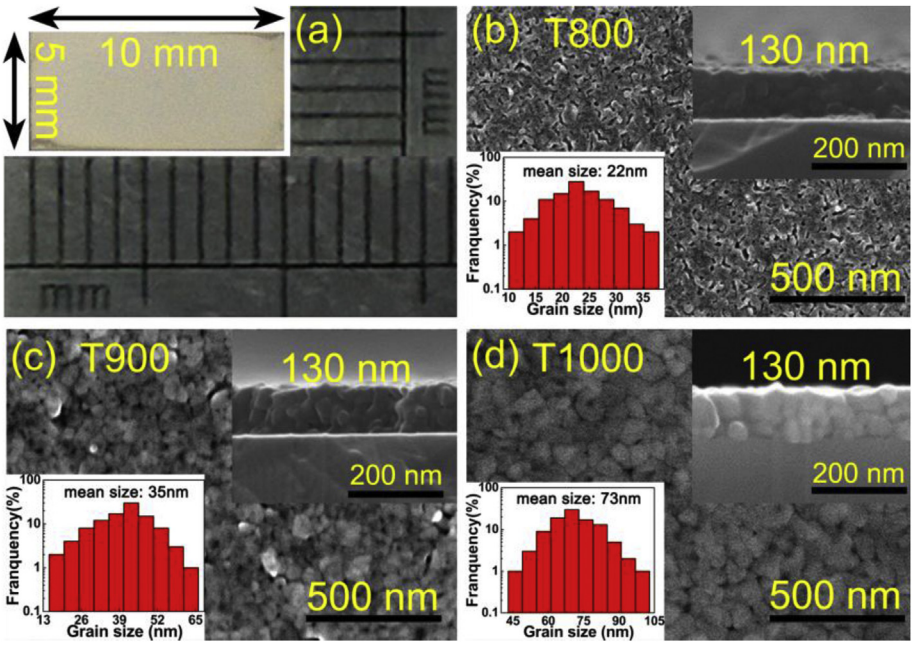

Fig. 2. (a) Photograph of the T_{1000} thin film. FE-SEM results of the derived CrN thin films annealed at different temperatures: (b) 800 °C, (c) 900 °C and (d) 1000 °C. The thickness and the history diagram of the grain size are shown in the corresponding insets.

as 22, 35, 73 nm for the T800, the T900 and the T1000 thin films, respectively. The increased grain size with annealing temperature increasing can be attributed to the enhanced grain growth [25]. As shown in the corresponding insets, the thin film thickness is determined to be ~130 nm from the cross-sectional FE-SEM measurements for all the prepared CrN thin films.

To further investigate the microstructures, high-resolution TEM (HRTEM) measurements are carried out and the results are shown in Fig. 3. The surface HRTEM results of the derived CrN thin films annealed at different temperatures are shown in Fig. 3(a), (c) and (e). With the increasing annealing temperature, the grain boundaries can be observed more clearly, indicating the improved crystalline quality. The average grain size increases with the increasing annealing temperature, confirming the FE-SEM results. The Selected Area Electron Diffraction (SAED) patterns are presented as diffraction rings as shown in the insets of Fig. 3(b), (d) and (f) for the T800, the T900 and the T1000, respectively. The diffraction rings from center to edge are indexed as (111), (200), (220), (311), (222) and (400) respectively, indicating the polycrystalline characteristics. With the increasing annealing temperature, the diffraction rings tend to become sharper, further confirming the enhancement of the crystalline quality.

3.2. Characterization of the N content variations

To investigate the N content variations in the CrN thin films, XPS measurements are performed and the results are shown in Fig. 4. The peaks centered at ~575 eV can be attributed to the Cr $2p_{3/2}$ and the asymmetric shape of the Cr 2p peak is originated from the Doniach-Sunjic effects [26]. The N peaks centered at ~ 396 eV can be attributed to the N $1s_{1/2}$, confirming the appearance of N element in the derived CrN thin films [27]. As reported previously, the binding energies of Cr 2p and N 1s are both decreased with N content increasing [28–30]. The decreases indicate that the attraction of the electrons surrounding the ionized Cr atom becomes less and less effective as the N content increasing. It also represents the order of decreasing neutralization of charge surrounding the Cr-cation and increasing neutralization of charge surrounding the N-anion in these films [30]. The binding energy of Cr $2p_{3/2}$ and N $1s_{1/2}$ is 574.92 and 396.45 eV for the T800, 574.82 and 396.40 eV for the T900 and 574.71 and 396.25 eV for the T1000, respectively, suggesting the increased N content with the increasing annealing temperature [27].

3.3. Electrical transport properties

To give the carrier concentration as well as the carrier mobility, the room-temperature Hall measurements are carried out. The results show that the carrier type is electron-type (n-type) as previously reported [15]. As shown in Fig. 5(a), the calculated electronic carrier concentration N_e and electron mobility μ_e are 9.44×10^{20} cm^{-3} and 1.17 cm^2 $V^{-1}s^{-1}$, 2.99×10^{21} cm^{-3} and 0.95 cm^2 $V\text{-}^1s^{-1}$, 3.08×10^{21} cm^{-3} and 2.52 cm^2 $V^{-1}s^{-1}$ for the T800, the T900 and the T1000, respectively. With the increasing annealing temperature, the increased N content will lead to an increased electronic carrier concentration. Meanwhile, the less grain boundary scattering, the enlarged grain size and the improved crystalline quality will lead to the improved electron mobility. However, the increase in carrier concentration will lead to a decrease in the mobility due to the enhanced electron-electron scattering [10]. Consequently, the combined effects lead to the enhanced carrier concentration with increasing annealing temperature, while the mobility is the lowest for the T900.

The temperature dependence of resistivity is shown in Fig. 5(b) and the measured current is 5 mA. It is seen that all the prepared CrN thin films show a semiconductor-like behavior with $d\rho/dT < 0$ within the measured temperature range of 5–350 K. The resistivity within the whole measured temperature range is decreased with the increasing annealing temperature. The resistivity at 300 K (ρ_{300K}) is 5.61, 2.18 and 0.79 mΩ cm for the T800, T900 and T1000, respectively, which is within the range of the previous reports for the epitaxial and polycrystalline CrN thin films [4,6,15–17]. With the increasing annealing temperature, the resistivity is decreased due to the increased N content, the improved crystalline quality as

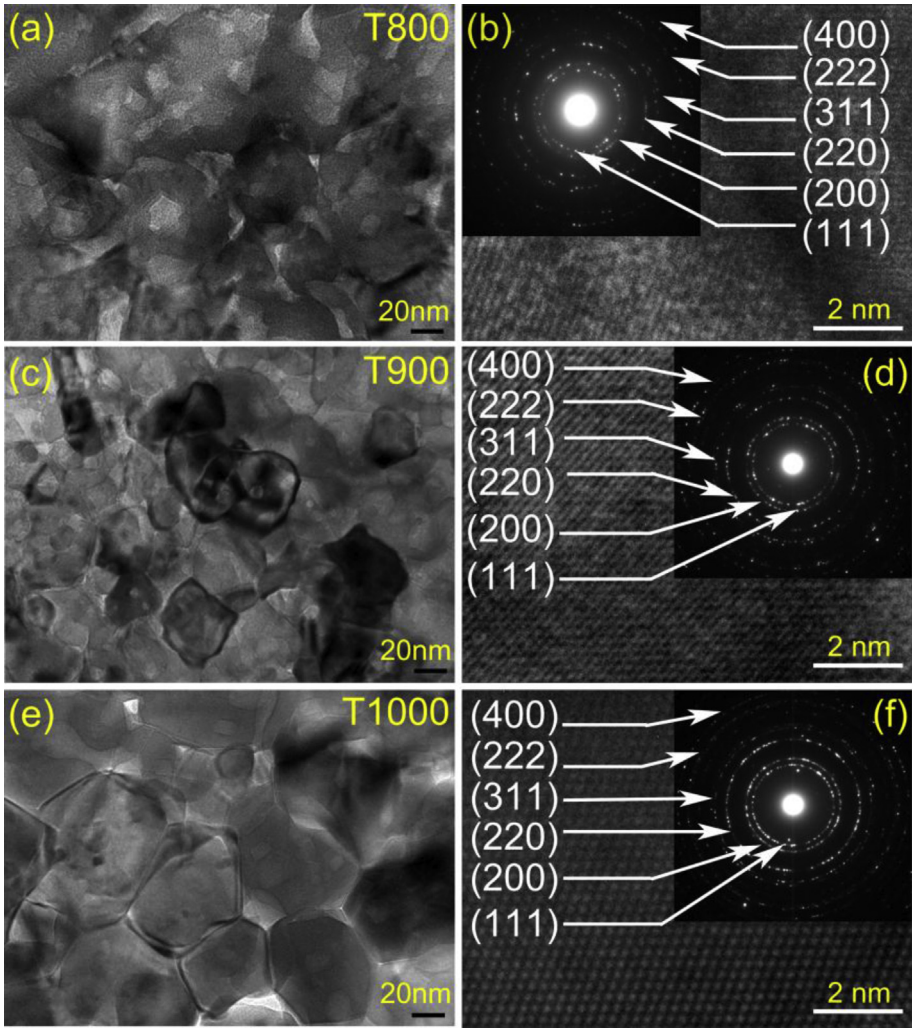

Fig. 3. Surface HRTEM results of the derived CrN thin films annealed at different temperatures: (a) 800 °C, (c) 900 °C and (e) 1000 °C. The surface lattice stripes of the corresponding thin films: (b) 800 °C, (d) 900 °C and (f) 1000 °C. The SAED patterns are shown in the corresponding insets.

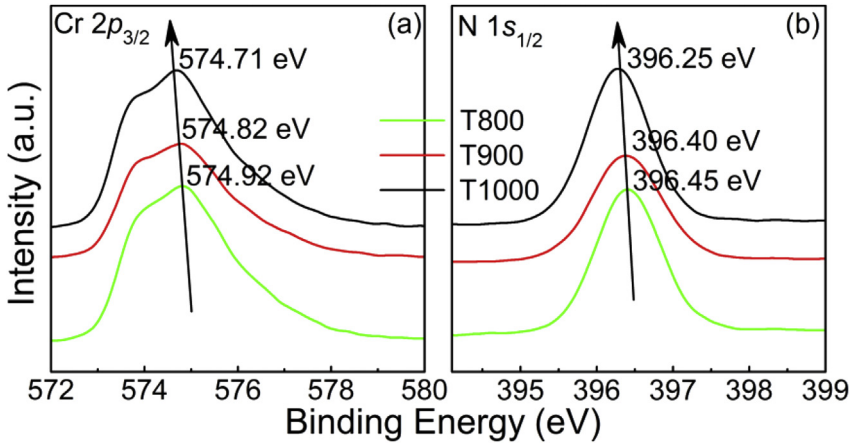

Fig. 4. XPS spectra of the CrN thin films annealed at different temperatures: (a) Cr 2*p* and (b) N 1*s*.

well as the enlarged grain size. Additionally, in CrN a characteristic is the presence of a phase transition from the high-temperature paramagnetic with rock-salt structure and space group *Fm-3m* to the low-temperature antiferromagnetic with orthorhombic structure and space group *Pnma* at the *Néel* temperature, showing a kink in resistivity [21,31]. The temperature of the resistivity kink is defined as T_K. To give the T_K, $d\rho/dT$ is calculated and the results are shown in the insets of Fig. 5(b). The obtained T_K is of 278, 279 and

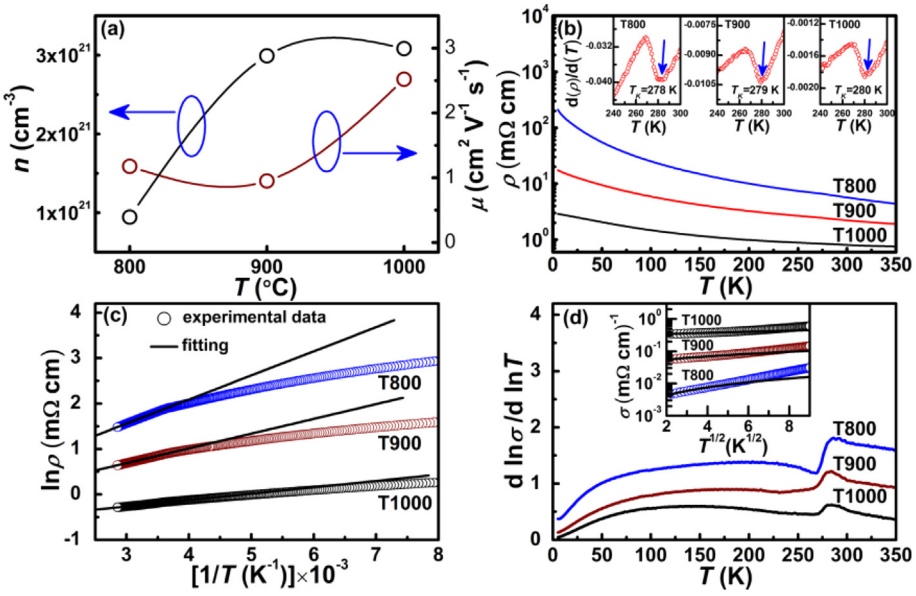

Fig. 5. (a) shows the variation of electron carrier concentration and electron mobility for CrN thin films annealed at different temperatures; (b) shows the temperature dependence of resistivity for the derived CrN thin films, the dρ/dT results to determine the T_K are shown in the insets. The transport fitting results of the CrN thin films annealed at different temperatures (c) in the region above T_K; (d) The plot of $d(ln\sigma)/d(lnT)$ vs T extrapolates to zero with $T\rightarrow 0$, a fit to the data is shown in the inset.

280 K for the T800, T900 and T1000 respectively, which is similar to previous reports [15,32,33].

To investigate the electrical transport mechanisms, the resistivity is fitted within different temperature ranges. For the temperature range above T_K, as shown in Fig. 5(c), it is observed that the resistivity can be well fitted by the thermal activation model $\rho(T) = \rho_0 e^{-(E_g/2k_BT)}$, where E_g is the band gap. The E_g is obtained as 91.4, 55.9 and 24.2 meV for the T800, T900 and T1000 respectively, which is similar to the previous report [33]. The decrease in E_g with annealing temperature can be attributed to the effects of N content, grain size and crystalline quality. As for the resistivity below T_K the thermal activation model cannot be fitted well the resistivity. It is reported that the resistivity behavior below T_K of CrN ceramics can be explained by the Möbius criterion [34]. The $d(ln\sigma)/d(lnT)$ extrapolates to zero with $T\rightarrow 0$ as the conductivity σ is a finite value at $T\rightarrow 0$ for metallic systems. In contrast, $d(ln\sigma)/d(lnT)$ will diverge as $T\rightarrow 0$ for systems with σ that follow an exponential dependence on T. As shown in Fig. 5(d), it is seen that the d(lnσ)/d(ln$T$) versus T tends to zero, suggesting the metallic characteristic of CrN [34]. In fact, as shown in the inset of Fig. 5(d), the conductivity can be fitted by $\sigma(T) = \sigma(0) + mT^{1/2}$, which suggests that CrN can be considered as a correlated metal in the presence of disorder [35,36].

3.4. Magnetoresistance at low temperatures under high magnetic fields

The *MR* at 10K for the three prepared CrN thin films is shown in Fig. 6(a) and the applied magnetic field direction is perpendicular to the film surface. It is seen that the *MR* value of the prepared CrN thin films is negative. Moreover, it is interesting to observe that the *MR* value is decreased with the increasing annealing temperature and the *MR* under 8.5 T is −0.33%, −0.24% and −0.11% for the T800, the T900 and the T1000, respectively. Generally, negative *MR* is observed in ferromagnetic materials due to the enhanced magnetic moment alignments, and positive *MR* is usually observed in other materials due to the Lorentz effects. In our experiments, the observed very small negative *MR* suggests the weak ferromagnetism in the prepared CrN, which may be attributed to the slight N deficiency. The slight N deficiency is possible to induce weak ferromagnetism as observed in previous reports in oxides due to vacancies [37,38]. Additionally, the N deficiency will be decreased with the increasing annealing temperature as confirmed from XPS measurements, which will lead to the decreased negative *MR* as observed in our experiments.

To further investigate the *MR* behaviors, the *MR* of the T1000 thin film is further measured under 14T at 2 and 4.2 K with the

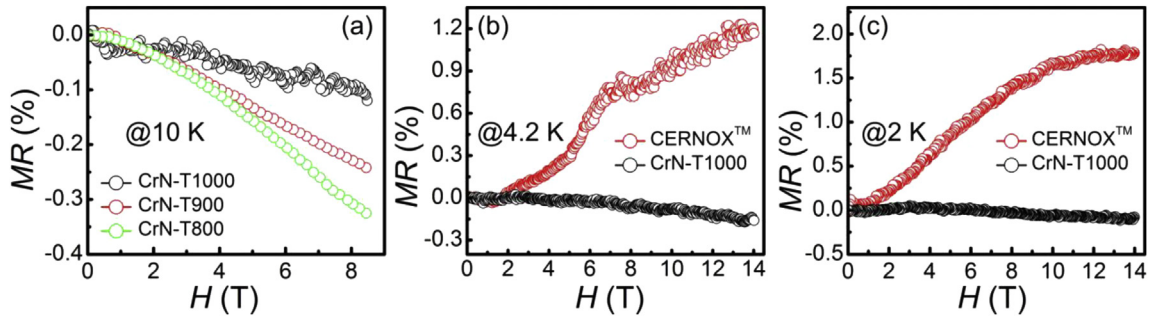

Fig. 6. (a)The *MR* at 10K for the three CrN thin films; (b) and (c) are the MR results of the T1000 thin film and the commercially CERNOX™ resistance thin film temperature sensors at 4.2 and 2K.

commercially CERNOX™ resistance thin film temperature sensors for a comparison and the results are shown in Fig. 6(b) and (c) at 4.2 and 2 K, respectively. It is seen that the *MR* value is negative and positive for the CrN and the CERNOX™ resistance thin film temperature sensor, respectively. It is interesting to observe that the absolute *MR* of the prepared CrN thin film is obviously lower than that of the CERNOX™ resistance thin film temperature sensor. The *MR* under 14T is −0.14% and 1.19% at 4.2 K and −0.10% and 1.78% at 2 K for the T1000 and CERNOX™, respectively. The absolute *MR* value under same applied magnetic fields is enhanced with the decreasing temperature for the CERNOX™ sensors due to the enhanced Lorentz force. As for our prepared CrN thin films, the absolute *MR* value under same applied magnetic fields is decreased with the decreasing measure temperature for the CrN thin films. With the decreasing measurement temperature, the Lorentz effects will be enhanced resulting in the enhanced positive *MR*. On the other hand, the negative *MR* will be enhanced due to the enhanced magnetic moment alignments. These two inverse effects might have led to the decreased negative MR as observed in our experiments, which needs further investigation.

4. Conclusion

CrN thin films have been successfully prepared by a modified chemical solution deposition processing. Annealing temperature effects on the growth mechanisms, microstructures, electrical tranport properties are investigated. Especially, ultra-low magnetoresistance is observed in the as-prepared CrN thin films, and the magnetoresistance value under 14T can be as low as −0.14% and −0.10% at 4.2 and 2 K, respectively. The CrN thin films can be considered as candidates for applications in temperature measuring at low temperatures and high magnetic fields. The achievement is a tremendous leap toward the utilization of chemical solution methods to enable widely fundamental investigation about the properties as well as provide a very simple and low-cost method to synthesis other novel nitride thin films.

Acknowledgements

This work was supported by the National Nature Science Foundation of China under Contract No. 11574321. H.M. Luo acknowledges the funding support from NSF CMMI-1131290.

References

[1] L.C. Zhou, F. Körmann, D. Holec, M. Bartosik, B. Grabowski, J. Neugebauer, P. Mayrhofer, Structural stability and thermodynamics of CrN magnetic phases from ab initio calculations and experiment, Phys. Rev. B 90 (2014) 184102.
[2] P. Eklund, S. Kerdsongpanya, B. Alling, Transition-metal-nitride-based thin films as novel energy harvesting materials, J. Mater. Chem. C 4 (2016) 3905–3914.
[3] X.Y. Zhang, J.S. Chawla, R.P. Deng, D. Gall, Epitaxial suppression of the metal-insulator transition in CrN, Phys. Rev. B 84 (2011) 073101.
[4] K. Inumaru, K. Koyama, N. Imo-oka, S. Yamanaka, Controlling the structural transition at the Néel point of CrN epitaxial thin films using epitaxial growth, Phys. Rev. B 75 (2007) 054416.
[5] C. Heinisch, P. Ramminger, H. Hutter, SIMS investigation of CrN sputter coatings, Anal. Bioanal. Chem. 374 (2002) 592–596.
[6] C. Constantin, M.B. Haiger, D. Ingram, A.R. Smith, Metal/semiconductor phase transition in chromium nitride (001) grown by rf-plasma-assisted molecular-beam epitaxy, Appl. Phys. Lett. 85 (2004) 6371–6373.
[7] A. Ney, R. Rajaram, S.S.P. Parkin, T. Kammermeier, S. Dhar, Magnetic properties of epitaxial CrN films, Appl. Phys. Lett. 89 (2006) 112504.
[8] V.M. Vishnyakov, V.I. Bachurin, K.F. Minnebaev, R. Valizadeh, D.G. Teer, J.S. Colligon, V.V. Vishnyakov, V.E. Yurasova, Ion assisted deposition of titanium chromium nitride, Thin Solid Films 497 (2006) 189–195.
[9] F.F. Lange, Chemical solution routes to single-crystal thin films, Science 273 (1996) 903–909.
[10] H.M. Luo, Y. Lin, H.Y. Wang, J.H. Lee, N.A. Suvorova, A.H. Mueller, A.K. Burrell, T.M. McCleskey, E. Bauer, I.O. Usov, M.E. Hawley, T.G. Holesinger, Q.X. Jia, A Chemical solution approach to epitaxial metal nitride thin films, Adv. Mater. 21 (2009) 193–197.
[11] G.F. Zou, M. Jain, H.H. Zhou, H.M. Luo, S.A. Baily, L. Civale, E. Bauer, T.M. McCleskey, A.K. Burrell, Q.X. Jia, Ultrathin epitaxial superconducting niobium nitride films grown by a chemical solution technique, Chem. Commun. (2008) 6022–6024.
[12] G. Subramanyam, M.W. Cole, N.X. Sun, T.S. Kalkur, N.M. Sbrockey, G.S. Tompa, X.M. Guo, C.L. Chen, S.P. Alpay, G.A. Rossetti, J.K. Dayal, L.Q. Chen, D.G. Schlom, Challenges and opportunities for multi-functional oxide thin films for voltage tunable radio frequency/microwave components, J. Appl. Phys. 114 (2013) 191301.
[13] Z.Z. Hui, X.W. Tang, D.F. Shao, H.C. Lei, J. Yang, W.H. Song, H.M. Luo, X.B. Zhu, Y.P. Sun, Epitaxial antiperovskite superconducting $CuNNi_3$ thin films synthesized by chemical solution deposition, Chem. Commun. 50 (2014) 12734.
[14] Z.Z. Hui, X.W. Tang, D.F. Shao, R.H. Wei, J. Yang, P. Tong, W.H. Song, X.B. Zhu, Y.P. Sun, Self-assembled c-axis oriented antiperovskite soft-magnetic $CuNCo_3$ thin films by chemical solution deposition, J. Mater. Chem. C 3 (2015) 4438–4444.
[15] C.X. Quintala, J.P. Podkaminer, M.N. Luckyanava, T.R. Paudel, E.L. Thies, D.A. Hillsberry, D.A. Tenne, E.Y. Tsymbal, G. Chen, C.B. Eom, F. Rivadulla, Epitaxial CrN thin films with high thermoelectric figure of merit, Adv. Mater. 27 (2015) 3032–3037.
[16] R. Sanjinés, O. Banakh, C. Rojas, P.E. Schmid, F. Lévy, Electronic properties of $Cr_{1-x}Al_xN$ thin films deposited by reactive magnetron sputtering, Thin Solid Films 420–421 (2002) 312–317.
[17] Y. Tsuchiya, K. Kosuge, Y. Ikeda, T. Shigematsu, S. Yamaguchi, N. Nakayama, Non-stoichiometry and antiferromagnetic phase transition of NaCl-type CrN thin films prepared by reactive sputtering, Mater. Trans. 37 (1996) 121–129.
[18] Z.Z. Hui, X.W. Tang, R.H. Wei, L. Hu, J. Yang, H.M. Luo, J.M. Dai, W.H. Song, X.Z. Liu, X.B. Zhu, Y.P. Sun, Facile chemical solution deposition of nanocrystalline CrN thin films with low magnetoresistance, RSC Adv. 4 (2014) 12568–12571.
[19] K. Satoh, Y. Kakehi, M. Uno, Y. Sakurai, T. Yotsuya, T. Ishida, Electrical properties of Cr-N films deposited by sputtering: application to cryogenic temperature sensors, Jpn. J. Appl. Phys. 51 (2012) 01AC07.
[20] T. Yotsuya, Y. Kakehi, T. Ishida, Thin film temperature sensor for cryogenic region with small magnetoresistance, Cryogenics 51 (2011) 546–549.
[21] J.D. Browne, P.R. Liddell, R. Street, T. Mills, An investigation of the antiferromagnetic transition of CrN, Phys. Stat. Sol. 1 (1970) 715–723.
[22] L. Li, Q. Zhen, R. Li, Nitridation of chromium powder in ammonia atmosphere, Int. J. Min. Metall. Mater. 22 (2015) 319–324.
[23] Y. Kido, G. Hasegawa, K. Kanamori, K. Nakanishi, Porous chromium-based ceramic monoliths: oxides (Cr_2O_3), nitrides (CrN), and carbides (Cr_3C_2), J. Mater. Chem. A 2 (2014) 745–752.
[24] M. Katsura, Thermodynamics of nitride and hydride formation by the reaction of metals with flowing NH_3, J. Alloys Comp. 182 (1992) 91–102.
[25] X.W. Tang, X.B. Zhu, J.M. Dai, J. Yang, L. Hu, L. Chen, X.D. Zhu, X.H. Li, H.F. Jiang, R.R. Zhang, Y.P. Sun, c-Axis oriented $SrMoO_4$ thin films by chemical solution deposition: self-assembled orientation, grain growth and photoluminescence properties, Acta Mater. 65 (2014) 287–294.
[26] E. Sacher, Asymmetries in transition metal XPS spectra: metal nanoparticle structure, and interaction with the graphene-structured substrate surface, Langmuir 26 (2010) 3807–3814.
[27] F. Rivadulla, M. Bañobre-López, C.X. Quintela, A. Piñeiro, V. Pardo, D. Baldomir, M.A. López-Quintela, J. Rivas, C.A. Ramos, H. Salva, J.S. Zhou, J.B. Goodenough, Reduction of the bulk modulus at high pressure in CrN, Nat. Mater. 8 (2009) 947–951.
[28] M. Chen, S. Wang, J.Z. Zhang, D.W. He, Y.S. Zhao, Synthesis of stoichiometric and bulk CrN through a solid-state ion-exchange reaction, Chem. Eur. J. 18 (2012) 15459–15463.
[29] I. Bertóti, M. Mohai, P.H. Mayrhofer, C. Mitterer, Surface chemical changes induced by low-energy ion bombardment in chromium nitride layers, Surf. Interface Anal. 34 (2002) 740–743.
[30] C. Emerya, A.R. Chourasia, P. Yashar, A study of CrN_x thin films by X-ray photoelectron spectroscopy, J. Electron Spectrosc. Relat. Phenom. 104 (1999) 91–97.
[31] L.M. Corliss, N. Elliott, J.M. Hastings, Antiferromagnetic structure of CrN, Phys. Rev. 117 (1960) 929–935.
[32] X.Y. Zhang, J.S. Chawla, R.P. Deng, D. Gall, Epitaxial suppression of the metal-insulator transition in CrN, Phys. Rev. B 84 (2011) 073101.
[33] P.A. Bhobe, A. Chainani, M. Taguchi, T. Takeuchi, R. Eguchi, M. Matsunami, K. Ishizaka, Y. Takata, M. Oura, Y. Senba, H. Ohashi, Y. Nishino, M. Yabashi, K. Tamasaku, T. Ishikawa, K. Takenaka, H. Takagi, S. Shin, Evidence for a correlated insulator to antiferromagnetic metal transition in CrN, Phys. Rev. Lett. 104 (2010) 236404.
[34] A. Mobius, Comment on metal-insulator-transition in amorphous $Si_{1-x}Cr_x$, Solid State Commun. 73 (1990) 215–219.
[35] P.A. Lee, T.V. Ramakrishnan, Disordered electronic systems, Rev. Mod. Phys. 57 (1985) 287.
[36] T.F. Rosenbaum, K. Andres, G.A. Thomas, P.A. Lee, Conductivity cusp in a disordered metal, Phys. Rev. Lett. 48 (1981) 568–571.
[37] M. Venkatesan, C.B. Fitzgerald, J.M.D. Coey, Unexpected magnetism in a dielectric oxide, Nature 430 (2004) 630.
[38] A.S. Foster, F. Lopez Gejo, A.L. Shluger, R.M. Nieminen, Vacancy and interstitial defects in hafnia, Phys. Rev. B 65 (2002) 174117.